

Decomposing Leftovers: Event, Path, and Site Residuals for a Small-Magnitude Anza Region GMPE

by Valerie Sahakian, Annemarie Baltay, Tom Hanks, Janine Buehler,
Frank Vernon, Debi Kilb, and Norman Abrahamson

Abstract Ground-motion prediction equations (GMPEs) are critical elements of probabilistic seismic hazard analysis (PSHA), as well as for other applications of ground motions. To isolate the path component for the purpose of building nonergodic GMPEs, we compute a regional GMPE using a large dataset of peak ground accelerations (PGAs) from small-magnitude earthquakes ($0.5 \leq M \leq 4.5$ with $>10,000$ events, yielding $\sim 120,000$ recordings) that occurred in 2013 centered around the ANZA seismic network (hypocentral distances ≤ 180 km) in southern California. We examine two separate methods of obtaining residuals from the observed and predicted ground motions: a pooled ordinary least-squares model and a mixed-effects maximum-likelihood model. Whereas the former is often used by the broader seismological community, the latter is widely used by the ground-motion and engineering seismology community. We confirm that mixed-effects models are the preferred and most statistically robust method to obtain event, path, and site residuals and discuss the reasoning behind this. Our results show that these methods yield different consequences for the uncertainty of the residuals, particularly for the event residuals. Finally, our results show no correlation (correlation coefficient [CC] < 0.03) between site residuals and the classic site-characterization term V_{S30} , the time-averaged shear-wave velocity in the top 30 m at a site. We propose that this is due to the relative homogeneity of the site response in the region and perhaps due to shortcomings in the formulation of V_{S30} and suggest applying the provided PGA site correction terms to future ground-motion studies for increased accuracy.

Electronic Supplement: Peak ground acceleration (PGA) dataset.

Introduction

There are many dimensions to earthquake hazard reduction and risk mitigation, and accurately estimating earthquake ground motion is one of the most important. For the engineering community, ground-motion prediction equations (GMPEs) are the principal means for estimating ground motion. In addition to hazard mapping applications and site-specific studies for building design, GMPEs are used in a variety of seismological problems, including earthquake early warning applications, rapid earthquake response (e.g., ShakeMap), and validation of physics-based models of ground-motion simulation. Because they are almost entirely empirical, even the most complete GMPEs embody considerable uncertainty of both the epistemic and aleatory types.

In particular, global or large-scale GMPEs are often less accurate and precise when applied on a local or regional scale. These discrepancies lead to large uncertainties or standard deviations in the median ground-motion model. Ground-motion uncertainties have plagued many seismological studies since

the very early days of local magnitude (Richter, 1935). Large uncertainties could result in the overprediction of high ground motions at low probabilities of exceedance (Bommer and Abrahamson, 2006; Hanks *et al.*, 2013; Stafford, 2014; Baltay *et al.*, 2017) and reduce the efficacy of the GMPE as an empirical baseline estimate for validation of ground-motion simulations or regional seismological studies. Nonergodic GMPEs or path-specific GMPEs can help ameliorate these problems (Anderson and Brune, 1999; Al Atik *et al.*, 2010). These models acknowledge that ground-motion distributions are not the same in time as in space by providing a ground-motion distribution for every path of interest as opposed to the same distribution for all possible paths.

To work toward fully nonergodic GMPEs that are valid for moderate- to large-magnitude events, we first need to study path effects that arise from small-magnitude events because this magnitude range contains the large volume of seismic data required for validating any physical relationships.

One way to test the usefulness of these events is empirical, in which the observed path effects for small earthquakes can be used in extrapolations to larger magnitude earthquakes. Another approach is to validate the path effects observed in 3D numerical simulations of earthquake rupture.

This article provides the basis for the first approach listed above. To study path effects from small-magnitude events, the path component of residuals must be isolated and compared against various physical properties or processes. Similar studies have been conducted with respect to source properties (Kotha *et al.*, 2016; Ameri *et al.*, 2017; Baltay *et al.*, 2017; Bindi *et al.*, 2017; Oth *et al.*, 2017). These studies examined how observed event terms or uncertainties can be correlated with independently determined stress-drop estimates, such that this information could put into GMPEs *a priori* to improve their predictive power (e.g., Baltay *et al.*, 2017). With respect to path effects, path residuals from an empirical GMPE decomposition may directly correlate with a seismic-velocity structure (or other earth material property). Path-specific GMPEs may then include information on the underlying velocity structure as physical predictive input parameters.

The goal of our larger study is to do just this. Developing an unbiased reference GMPE for these small-magnitude data is a first requirement because GMPEs developed from other datasets will not be sufficient to appropriately describe this region and magnitude range. Furthermore, to correlate path residuals with a velocity or other earth-material structure requires decomposition of the total residuals and uncertainty of a GMPE into the individual contributions arising from the residuals for the source (event), path, and site. It is difficult to separate these components, in particular for imbalanced datasets. The method with which these residuals and uncertainties are decomposed can also affect the results and is discussed in this article.

We begin by developing a regional PGA GMPE for small to moderate magnitudes ($0.5 \leq M \leq 4.5$) in the southern California region using a dense seismic network and a large catalog of earthquake waveform recordings. The zero-biased, small-magnitude GMPE is necessary as a reference model to remove average ground-motion scaling and isolate path effects. Additionally, it provides a model for regional, seismological studies and is important in constraining the hazard from small- to moderate-magnitude events (Chiou *et al.*, 2010; Beauval *et al.*, 2012; Atkinson and Morrison, 2014; Atkinson, 2015; Baltay *et al.*, 2017). Furthermore, because small-magnitude events in the southern California region are so often studied, findings from this GMPE study can be used by seismologists to better constrain or understand their own analysis (e.g., Kilb *et al.*, 2012; Trugman and Shearer, 2017). In a companion study, we use this GMPE and the multitude of small-magnitude recordings, together with high-resolution seismic-velocity models, to demonstrate a causal connection between the empirical GMPE path residuals and the velocity model (Sahakian *et al.*, 2016).

Then, we use this GMPE to illustrate two methods of obtaining residuals and event, path, and site terms for the GMPE: the pooled ordinary least-squares (POLS) and mixed-effects maximum-likelihood estimation (MLE) approach. Using these two different methods, we explore some of the implications of each method on the event, site, and in particular path terms, as well as the correlation and inclusion of regional parameters or physical processes into GMPEs. The differences between and implications of these methods have been explored by Stafford (2014) and Kotha *et al.* (2017); in this article, we bring these matters to the broader seismological community beyond engineering seismology.

Methods: Data, GMPE Development, and Residual Determination

The southern California region is well positioned for the purposes of this study because it exhibits high levels of seismic activity (Hardebeck and Hauksson, 2001), with dense continuous seismic networks that have been in place for decades (Berger *et al.*, 1984; Vernon, 1989). In 2013 alone, more than 10,000 events in southern California were recorded and cataloged (Fig. 1). This allows for the formation of a large database of seismic recordings, which we can use to both test the development of regional GMPEs and study the effects of various methods for computing residuals. This region has also been studied extensively with respect to physical properties and processes that may affect ground motions, including regional velocity models (Allam *et al.*, 2014; Fang *et al.*, 2016), attenuation structure (Hauksson and Shearer, 2006), and geologic structure (Plesch *et al.*, 2007; Shaw *et al.*, 2015) as well as models of fault-slip rate (Bennett *et al.*, 1996) and models of ground motion (Kurzon *et al.*, 2014).

When using GMPE residuals to glean information about regional seismological characteristics and phenomena, the estimates of the event, path, and site residuals (and their variability) should be as accurate as possible. Several possible statistical methods are used to obtain estimates of GMPE residuals. A widely used seismological framework for obtaining these (e.g., Baltay *et al.*, 2017) is the POLS method, which computes the mean of all GMPE residuals for each event and then for each site. This POLS regression method implies that the data and residuals for various events and sites are independent and represented by a Gaussian distribution (Greene, 2012); that is, nearby sites will demonstrate completely independent ground-motion variability. In contrast, a mixed-effects MLE (or restricted maximum-likelihood [REML]) approach, widely used by earthquake engineers and ground-motion seismologists, computes the residuals simultaneously with the underlying variances of the event and site residuals. This method assumes that the data and uncertainties are correlated (e.g., Abrahamson and Youngs, 1992; i.e., all recordings of a particular event will be correlated, as will recordings at a single site) and solves for the covariance between the data and uncertainties. Both methods contain assumptions and implications affecting the resulting residuals and their covariances.

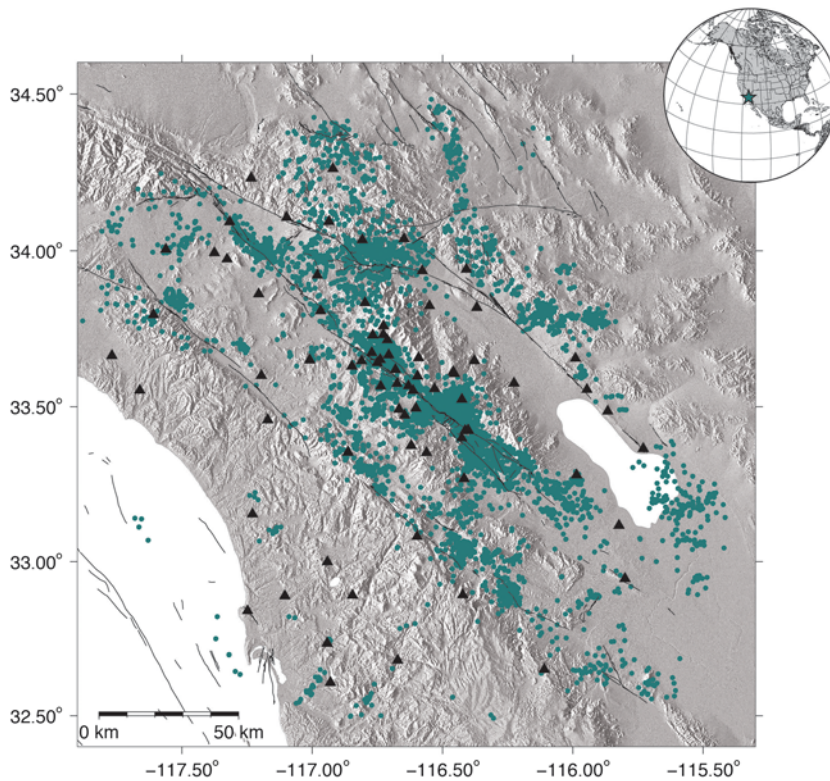


Figure 1. Regional map of our study region, including $>10,000$ small-magnitude ($0.5 \leq M \leq 4.5$) events (dots) and seismic stations (triangles). U.S. Geological Survey mapped Holocene–Latest Pleistocene faults are shown as black lines. The star in the inset shows the geographic location of the main map. The color version of this figure is available only in the electronic edition.

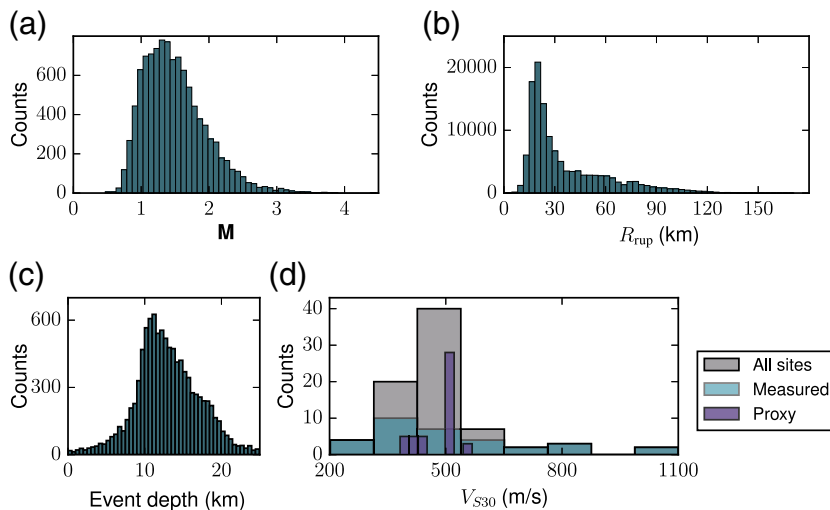


Figure 2. (a) Histogram of moment magnitude distribution of unique events in the dataset; the largest event in our database is M 4.5. (b) Histogram of R_{rup} distances for all recording in the dataset. (c) Histogram of event depths for each earthquake in the database. (d) Histogram of the V_{S30} distribution for the 78 stations in this study, all stations with measured V_{S30} , and all stations with a proxy V_{S30} . The color version of this figure is available only in the electronic edition.

Data

Our dataset contains more than 120,000 recordings of earthquakes recorded in the year 2013. It is composed of more than 10,000 events recorded on a minimum of 5 stations, within a 78-station array. The majority of events in our catalog are small magnitude $1 < M < 3$ with the largest $M \sim 4.5$ and recorded at distances (R_{rup} , closest distance to rupture) of $R_{rup} < 180$ km (Figs. 2 and 3). No events larger than M 4.5 are in the database because none occurred during the year 2013, and very few of the events are $M > 3$. The 78 stations in this dataset are from the ANZA (AZ), San Jacinto Fault Zone (SJFZ), Caltech (CI), UC Santa Barbara (UCSB), and Plate Boundary Observatory (PBO) networks. The majority of seismic instruments in this study are STS-2s with Quanterra digitizers. V_{S30} is included as a measure of site effects. V_{S30} is the time-averaged shear-wave velocity in the top 30 m of the Earth's surface and is a proxy for site amplification. Site V_{S30} values (Fig. 2) have been measured at 32 of the 78 stations (Yong *et al.*, 2016), and when measured values are not available, we use estimated values at the remaining 46 stations via a terrain-based proxy method (Yong *et al.*, 2012). All waveforms are high-pass filtered at 0.5 Hz to avoid noise contamination but still preserve peak amplitudes for events in our magnitude range. All waveforms have either analyst-selected P - and S -wave arrivals or theoretically computed arrivals (Ross *et al.*, 2016), with a 30-s time window after the P -wave arrival used for the maximum amplitude measurements. Peak ground acceleration (PGA) is computed as the geometric average of the peak acceleration from the time series on the two horizontal channels at each station; RotD50 could be used instead of the geometric mean to reduce uncertainty; however, previous studies found little reduction using this parameter (Beyer and Bommer, 2006; Boore, 2006). Finally, the signal-to-noise ratio is computed as the PGA in the signal window divided by the maximum amplitude in the noise window before the P -wave arrival. In this study, we do not include peak ground velocity (PGV) or effective amplitude spectra (EAS, which is the quadratic mean of the Fourier amplitude spectrum of the two horizontal components; Bayless and Abrahamson, 2018).

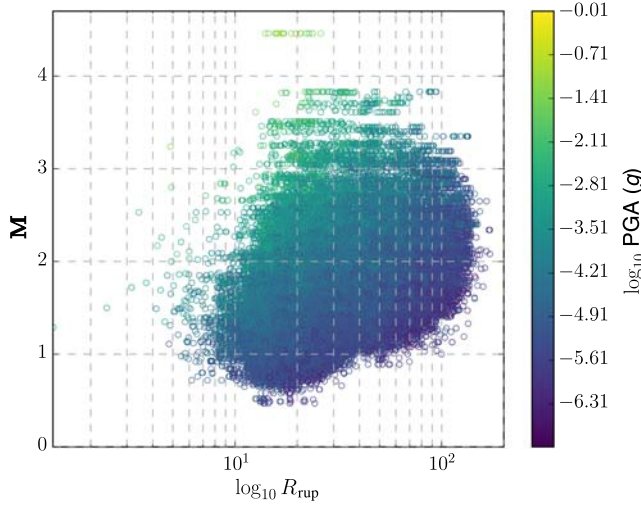


Figure 3. Magnitude versus distance for this dataset. Recordings are shaded by \log_{10} PGA (peak ground acceleration). The color version of this figure is available only in the electronic edition.

GMPE Development and Residual Computation

The functional form we use here is a simplified version of [Abrahamson et al. \(2014\)](#) with either six terms:

$$f(M, R_{\text{rup}}) = a_1 + a_2 M + a_3 (8.5 - M)^2 + a_4 \ln(R) + a_5 R_{\text{rup}} + a_6 \ln\left(\frac{V_{S30}}{V_{\text{ref}}}\right), \quad (1)$$

or with five terms, omitting the V_{S30} term:

$$f(M, R_{\text{rup}}) = a_1 + a_2 M + a_3 (8.5 - M)^2 + a_4 \ln(R) + a_5 R_{\text{rup}}, \quad (2)$$

in which

$$R = \sqrt{R_{\text{rup}}^2 + c^2}. \quad (3)$$

The regressed ground-motion intensity is $\ln(\text{PGA})$, in which PGA is peak ground acceleration in units of g . R_{rup} is equivalent to the hypocentral distance for these small earthquakes, and c is the finite-fault dimension factor, taken here to be a constant 4.5 ([Abrahamson et al., 2014](#)). The first term a_1 is simply an overall constant or intercept; a_2 and a_3 account for the magnitude dependence of PGA; a_4 is the geometric spreading coefficient; a_5 is the anelastic attenuation term; and a_6 is the linear V_{S30} parameter. V_{S30} in this region is fairly homogeneous (with the majority of stations between ~ 300 and 700 m/s). Because of this homogeneity and the fact that nonlinear effects are not of concern for such small-magnitude events, we consider only a linear V_{S30} relation.

The observed ground motions may be written as a combination of the GMPE prediction $f(M, R_{\text{rup}})_{ij}$, and a total residual δ_{ij} , for any event i and station j :

$$y_{ij} = f(M, R_{\text{rup}})_{ij} + \delta_{ij}. \quad (4)$$

The total residual can be decomposed into components that represent contributions from the source (event), path, and site. It is traditionally considered to first be decomposed into δE_i , the average event-term (also called between-event or interevent) residual, and the within-event (or intraevent) residual δW_{ij} , for the recording of event i at station j :

$$\delta_{ij} = \delta E_i + \delta W_{ij}. \quad (5)$$

The within-event residual is a combination of a site-term residual δS_j at station j , path-term residual δP_{ij} , and the remaining random residual for recording of earthquake i at station j , δW_{ij}^0 :

$$\delta W_{ij} = \delta S_j + \delta P_{ij} + \delta W_{ij}^0. \quad (6)$$

Because we cannot separate out the path residual from random residual δW_{ij}^0 , we combine them to be δWS_{ij} and hereafter call this the path term or path residual, using the same notation as [Baltay et al. \(2017\)](#).

The standard deviation of the total residual $\text{st.dev.}(\delta_{ij}) = \sigma$ can itself be decomposed as

$$\sigma^2 = \tau^2 + \phi_S^2 + \phi_{SS}^2, \quad (7)$$

in which τ is the standard deviation of the event terms for all unique events; ϕ_S is the standard deviation of site terms for all unique sites; and ϕ_{SS} the single-station standard deviation, a combination of the path and random uncertainty. In the future, we will ideally move toward decomposing this into a path standard deviation and a remaining component.

The POLS method of GMPE development first inverts for the coefficients in equation (1) or (2) with a least-squares inversion, with no grouping or weighting of the events or stations (pooling them all together), and then decomposes the residuals into event, path, and site terms (see [Wang and Jordan, 2014](#); [Baltay et al., 2017](#), for details). The event term δE_i is calculated as the mean of all δ_{ij} per event (in which n_i is the number of stations recording event i):

$$\delta E_{i\text{-POLS}} = \frac{1}{n_i} \sum_{j=1}^{n_i} \delta_{ij}. \quad (8)$$

The within-event residual δW_{ij} is calculated as $\delta W_{ij} = \delta_{ij} - \delta E_i$ and δS_j is then the mean of δW_{ij} at any one station (in which m_j is the number of events recorded on station j):

$$\delta S_{j\text{-POLS}} = \frac{1}{m_j} \sum_{i=1}^{m_j} (\delta_{ij} - \delta E_i). \quad (9)$$

The path term is assumed to be the remaining residual δWS_{ij} , which is in fact some combination of path and aleatory residuals.

The disadvantage of the POLS method is that the relative uncertainties of the event and site and the covariance of the data are not taken into consideration in the GMPE computation (Stafford, 2014). For example, every database with a certain population of events and stations will present its own unique associated uncertainties (τ , ϕ_S , ϕ_{SS}) and biases, different from another data population. Without accounting for the trade-offs of these uncertainties during the step of inverting for the GMPE coefficients, the coefficients may acquire some of the database's unique event and site uncertainty, and the event and site terms themselves will not reflect how well constrained (or well recorded) each individual event and site is. In addition, the nonweighted, grouped least-squares regression (and ensuing residuals) assumes that the individual data and their uncertainties are independent, but they clearly are not (e.g., recordings at the same site should be correlated as they share similar site effects).

Alternatively, an MLE or REML mixed-effects model will allow both the GMPE coefficients and event and site terms to be inverted for simultaneously, as well as all their respective uncertainties. In this model, all of the GMPE coefficients are considered fixed effects because their relationship to the predictive parameter is constant regardless of the selected population of data. The selected populations of events and sites, however, will affect the uncertainty of the model differently with every population. In this case, the event and site terms are then considered random effects. In a mixed-effects model, the functional form then becomes

$$\ln y_{ij} = f(M, R_{rup})_{ij} + \delta E_i + \delta S_j + \delta WS_{ij}, \quad (10)$$

in which the fixed effects for a recording of the i th earthquake and j th station are the coefficients a_1 – a_5 (or a_6), and the random effects δE_i and δS_j are the event term and site term, respectively. The remaining residual per recording for a mixed-effects model is then δWS_{ij} , which is a combination of the path term δP_{ij} and aleatory component

$$\delta WS_{ij} = \delta P_{ij} + \delta W_{ij}^0, \quad (11)$$

in which δP_{ij} is the path term for the i th earthquake and j th station and δW_{ij}^0 is the random component of the residuals. In the mixed-effects MLE approach, as in the POLS method, what we hereafter call the path-term residual is

$$\delta WS_{ij} = \ln y_{ij} - f(M, R_{rup})_{ij} - \delta E_i - \delta S_j. \quad (12)$$

Random effects require grouping factors, so δE_i is grouped by event number and δS_j by station name or number. With an adequate grouping factor, the path term δWS_{ij} could also be included as a random effect (i.e., Walling, 2009), but for this study, we do not explore a potential grouping or classification method for the paths. We also do not explore grouping events by source location (e.g., for repeating events, position along the fault), but this would be useful for investigating possible source effects in a region. Additionally, it is possible

to allow for interaction among grouping factors; however, we do not because events should not depend on sites. The fixed and random effects are solved for with a maximum-likelihood algorithm using the R lme4 package, and the values of each event and site term are determined through this algorithm with the best linear unbiased predictors method (Pinheiro and Bates, 2000; Bates *et al.*, 2015).

Results

We apply both of the methods described to our data and compute models and residuals for functional forms with and without the V_{S30} term (5 and 6 term models) to explore the relevancy of the V_{S30} term with this database. In several instances, the coefficients obtained through a purely mixed-effects inversion were unrealistic in nature, in particular for the geometrical spreading and intrinsic attenuation terms (a_4 and a_5), because these terms are highly correlated. In these instances, we explored models with certain coefficients prescribed and the remaining terms inverted for as fixed effects.

The coefficients for each of our models can be found in Table 1, along with a variance reduction (VR) for goodness of fit (equation 10; Melgar *et al.*, 2012). The uncertainties (standard deviations) for total residuals, event, path, and site terms as described earlier are listed in Table 2. The results are partitioned into two categories: (1) models with six coefficients (including a V_{S30} term) and (2) models with only five coefficients (no V_{S30} term).

Overview

From a seismological perspective, we expect the derived parameters to be consistent with the underlying physics. For these small-magnitude events ($M < 3$), the scaling of \log_{10} PGA should be $M \sim 1.5$ because of saturation of the apparent corner frequency (Hanks and Boore, 1984; Baltay and Hanks, 2014), and the slope with M should decrease with increasing magnitude. Geometrical spreading in a homogeneous elastic half-space is expected to be equivalent to $1/R$, equating to a value of -1.0 for a_4 , and a_5 should be related to the anelastic attenuation parameter Q approximated as $a_5 = \frac{-\pi f}{Q\beta}$, in which the frequency f is the frequency of interest in the recording (see more discussion of Q below). For the site response, we expect a linear regime for these small-magnitude events. This is based on prior studies (e.g., Seyhan and Stewart, 2014) that find a linear V_{S30} term coefficient (a_6) of -0.6 for PGA. Because V_{S30} is the average shear-wave velocity in the top 30 m of the Earth's surface, this coefficient implies that smaller values of V_{S30} (i.e., softer sediments) cause amplification; shaking should be greater on softer unconsolidated material than on hard rock. The intercept serves as an overall adjustment to the dataset.

The first category of models, six-coefficient models, contains six models, labeled A6–D6 (Table 1). The second category, with five-coefficient models, contains seven models, labeled A5–G5 (Table 1). Models A6 and A5 are the least-

Table 1
Model Coefficients

Model Name	Number of Terms	Model Comments	VR (%)	a_1	a_2	a_3	a_4	a_5	a_6
A6	6	Single mean	99.4	2.45	0.42	-0.17	-1.73	-0.0056	0.56
B6	6	ME (invert all)	99.9	4.89	0.23	-0.17	-2.44	0.0096	0.023
C6	6	ME (set a_2 - a_5)	96.8	2.33	0.42*	-0.17*	-1.73*	-0.0056*	0.13
C6_site	6	ME (set a_2 - a_6)	97.3	2.56	0.42*	-0.17*	-1.73*	-0.0056*	0.56*
D6	6	ME (set a_4 and a_5)	99.3	-0.26	0.84	-0.13	-1.73*	-0.0056*	0.0061
D6_site	6	ME (set a_4 - a_6)	99.3	-0.0059	0.84	-0.13	-1.73*	-0.0056*	0.56*
A5	5	Single mean	99.3	2.76	0.31	-0.18	-1.72	-0.0059	N/A
B5	5	ME (invert all)	99.9	4.87	0.23	-0.18	-2.44	0.0096	N/A
C5	5	ME (set a_2 - a_5)	97.8	2.85	0.31*	-0.18*	-1.72*	-0.0059*	N/A
D5	5	ME (set a_4 and a_5)	99.4	-0.34	0.85	-0.13	-1.72*	-0.0059*	N/A
E5	5	ME (set $a_4 = -1.0$)	99.7	-5.69	1.48	-0.08	-1.0 [†]	-0.02	N/A
F5	5	ME (set $a_4 = -1.2$)	99.6	-4.23	1.31	-0.09	-1.2 [†]	-0.02	N/A
G5	5	ME (set $a_4 = -1.5$)	99.5	-2.03	1.05	-0.11	-1.5 [†]	-0.01	N/A

ME, mixed effects; VR, variance reduction.

*Coefficients set from the corresponding POLS inversion.

[†]Coefficients set according to the value shown.

Table 2
Models and Their Resulting Uncertainties

Model Name	Number of Terms	Model Comments	δ_{ij} Mean	σ	δE_i Mean	τ	δS_j Mean	ϕ_S	δWS_{ij} Mean	ϕ_{SS}
A6	6	Single mean	0	0.9	-0.031	0.48	0.08	0.65	0	0.46
B6	6	ME (invert all)	0	0.88	0	0.38	0	0.67	0	0.42
C6	6	ME (set a_2 - a_5)	0	0.87	0	0.35	0	0.67	0	0.43
C6_site	6	ME (set a_2 - a_6)	0	0.88	0	0.35	0	0.68	0	0.43
D6	6	ME (set a_4 and a_5)	0	0.86	0	0.35	0	0.66	0	0.43
D6_site	6	ME (set a_4 - a_6)	0	0.88	0	0.35	0	0.68	0	0.43
A5	5	Single mean	0	0.91	-0.032	0.47	0.05	0.64	0	0.46
B5	5	ME (invert all)	0	0.87	0	0.38	0	0.66	0	0.42
C5	5	ME (set a_2 - a_5)	0	0.87	0	0.35	0	0.67	0	0.43
D5	5	ME (set a_4 and a_5)	0	0.87	0	0.35	0	0.67	0	0.43
E5	5	ME (set $a_4 = -1.0$)	0	0.88	0	0.34	0	0.67	0	0.45
F5	5	ME (set $a_4 = -1.2$)	0	0.87	0	0.34	0	0.67	0	0.44
G5	5	ME (set $a_4 = -1.5$)	0	0.86	0	0.34	0	0.66	0	0.43

Six-term models include a V_{S30} term; five-term models do not. δ_{ij} mean, mean of the total residuals; σ , standard deviation of the total residuals; δE_i mean, mean of the unique event terms; τ , standard deviation of the unique event terms; δS_j mean, mean of the unique site terms; ϕ_S , standard deviation of the unique site terms; δWS_{ij} mean, mean of the path (path + aleatory) terms; ϕ_{SS} , standard deviation of the unique path (path + aleatory) terms.

squares inversion and single-mean models; all other models are mixed-effects models. In our models, we find that the coefficients a_1 - a_5 in the least-squares regression models A6 and A5 are to some degree realistic in their physical representation: a_5 , the intrinsic attenuation term, exhibits a negative coefficient; a_4 , the geometrical spreading term, is computed to be approximately -1.7 in both A6 and A5, stronger than previous studies but much closer to a seismologically derived value than what the mixed-effects models B6 and B5 (with all coefficients inverted for) yield. The source term coefficients a_2 and a_3 vary from those in recent Next Generation Attenuation-West2 (NGA-West2) GMPEs (e.g., Abrahamson *et al.*, 2014) because steeper slopes are expected for these smaller magnitudes.

Here, we define uncertainties to be similar if they are within 0.03 natural log units apart because this is approxi-

mately equal to the standard deviation of uncertainties between models such as in NGA-West2 (Gregor *et al.*, 2014). The total uncertainty and event-term uncertainty (σ and τ) for least-squares A6 and A5 are similar to each other and greater than those in their related mixed-effects models (B6-D6_site, and B5-G5); the site and path uncertainties (ϕ_S and ϕ_P) are similar between A6 and A5 and slightly smaller than the mixed-effects counterparts (0.66-0.68). POLS models exhibit a nonzero mean event and site term but zero value of the mean path term. This is because the mixed-effects approach effectually minimizes the means of the random effects populations; however, the POLS model does not weight the inversion based on the representation of each event and site, thus leading to a nonzero mean of the unique event and site terms for the POLS.

Comparison between 6 and 5 Coefficient Models

Models B6 and B5 are mixed-effects inversions, inverting for coefficients for all terms (a_1 – a_5). The resulting coefficients are very similar. Models C6 and C5 are a mixed-effects inversion run by setting the a_2 – a_5 coefficients to be equal to the least-squares inversion solution, thus only inverting for a_1 and a_6 , and a_1 , respectively. Because the POLS model coefficients vary between least-squares A6 and A5, so do a_2 – a_5 between mixed-effects models C6 and C5 (in which a_2 – a_5 are set from models A6 and A5, respectively); however, the uncertainties remain virtually the same (within 0.02 natural log units). Model C6_{site} sets coefficients a_2 – a_6 from model A6's values. It is similar to model C5; however, in C6_{site}, the V_{S30} coefficient a_6 is also set from the least-squares inversion A6; thus, the intercept and VR varies between C6_{site} and C5. The site standard deviation are only marginally different.

Model D6 (attenuation terms a_4 and a_5 fixed from least-squares model A6) may be compared with D5 (a_4 and a_5 set from least-squares model A5) because both of these models set the a_4 and a_5 coefficients from their associated least-squares inversions. In this way, we are inverting for all intercept and magnitude terms, as well as the site-term coefficient in the case of D6. Between D6 and D5, the magnitude terms a_2 and a_3 are virtually the same, though the intercept varies (and of course a_4 and a_5 vary too). The uncertainties as well as individual site terms are very similar between these two models. D6_{site} is a model computed by setting the a_4 , a_5 , and a_6 terms from the associated least-squares inversion, inverting for the intercept and magnitude term. Its coefficients and uncertainties vary little from models D6 and D5.

In all of the aforementioned models, the geometrical spreading term a_4 exhibited large negative values (< -1.7). Traditionally, geometrical spreading is considered to be $1/R$, for which a_4 would be -1.0 . Mixed-effects models E5, F5, and G5 were devised to explore the possibility of model convergence if the geometrical spreading term were less than -1.7 and investigate the effects of this on other parameters such as the intrinsic attenuation coefficient a_5 . All of these models invert for coefficients a_1 – a_3 and a_5 . Model E5 sets $a_4 = -1.0$, model F5 sets $a_4 = -1.2$, and model G5 sets $a_4 = -1.5$. In all of these models, the intrinsic attenuation coefficient a_5 is more negative than all other models: $a_5 = -0.02$ for models E5 and F5 with $a_4 = -1.0$ and -1.2 , respectively, and $a_5 = -0.01$ for model G5 with $a_4 = -1.5$. These results show that as a_4 approaches 0, a_5 becomes more negative, as well as a_1 (-5.69 , -4.23 , and -2.03 for models E5, F5, and G5, respectively). The magnitude coefficients a_2 and a_3 are relatively stable between these models.

Site Terms and V_{S30}

In all six-coefficient models, A6–D6_{site}, the V_{S30} term is positive, which is inconsistent with traditional results that low V_{S30} values will amplify ground motions (Seyhan and Stewart, 2014). None of our models show a correlation between site terms and V_{S30} values—they all exhibit correlation coefficients

(Pearson's r -values) of less than 0.03 absolute value (Fig. 4). Additionally, there is no significant difference in correlation in this dataset between site terms and V_{S30} for sites with a measured versus terrain-based proxy V_{S30} (Fig. 4c).

The site uncertainty is approximately the same, $\phi_s = 0.66$, 0.67 , and 0.68 for D6, D5, and D6_{site}, respectively. Even though model D6 includes a V_{S30} term in its functional form and model D5 does not, the site terms themselves are virtually the same among these models, with only very slight differences (< 0.01 natural log units; Fig. 4). The V_{S30} term coefficient a_6 is nearly zero in model D6 (similar to model D5 because the absence of a V_{S30} term is the same as a zero V_{S30} term coefficient). However, the intercept varies between these two models.

In model D6_{site}, the a_6 (V_{S30} term) coefficient is set from the least-squares model A6, where it is strongly positive. Because this essentially corrects the data with a high ground motion to high V_{S30} relationship, the site terms for model D6_{site} show a weak negative correlation— $r = -0.23$ —with both V_{S30} and $\ln(V_{S30})$, closer to what would be expected in a model with no V_{S30} term (Fig. 4a,b). However, model D5 (with no V_{S30} term) shows no correlation between the site terms and either V_{S30} or $\ln(V_{S30})$, for either measured or inferred V_{S30} . Assuming a statistical power of 0.90 and significance level of 0.05, a correlation between $\ln(V_{S30})$ and the site terms that is implied by many GMPEs would require a minimum of 68 stations, which we have here (with 78 stations in our study). Assuming the small correlation we observe, -0.03 at most, a sample size of 11,677 stations would be necessary to see the same statistical power of 0.90. These models indicate that this population of sites does not show a convincing (if any) relationship between PGA and V_{S30} .

Discussion

Physical Meaning of Our Preferred Model

The preferred model of this study is model F5: a mixed-effects model with geometric spreading coefficient a_4 set to -1.2 (i.e., $1/R^{1.2}$), inverting for the remaining coefficients (Fig. 5). We chose a five-coefficient model with no V_{S30} term because of the lack of correlation of V_{S30} and site terms regardless of model parameters (Table 2). Steidl (2000) finds a similar result of a weak to no correlation between V_{S30} and empirical site terms, and thus we prefer this five-coefficient model. The overall uncertainty for this model is $\sigma = 0.87$, the geometrical spreading and intrinsic attenuation coefficients are representative of known physical processes, and the magnitude terms also seismologically preferred because they yield a slope approaching **M** 1.5 at smaller magnitudes and decreasing with larger magnitudes.

Because the fit of several of the models is very similar (i.e., large variance reductions; Table 1), we rely on independent seismological information to choose a reasonable model based on the physical implications of the various coefficients. For these considerations, we look to the distance-dependent

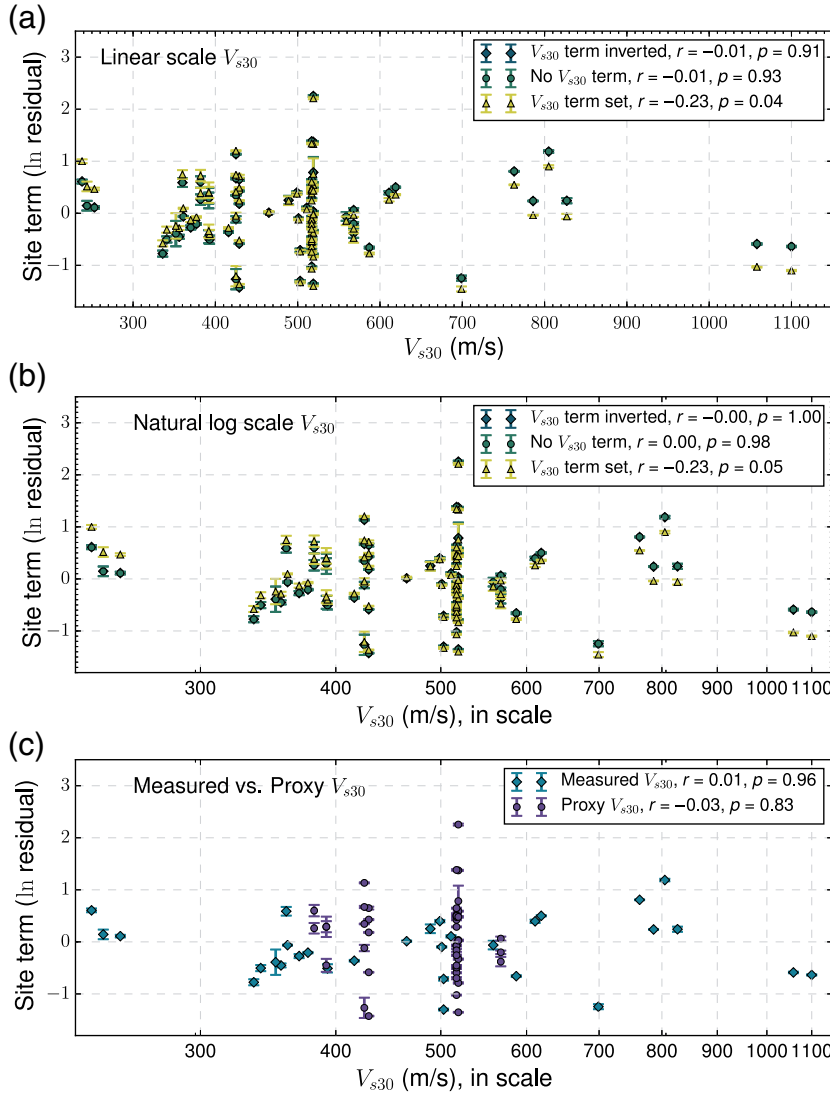


Figure 4. Site terms versus V_{S30} with site standard error as bars for three models, E6 (V_{S30} term inverted), D5 (no V_{S30} term), and F6 (V_{S30} term set from least-squares inversion), and for a single model with measured versus proxy V_{S30} values. (a) V_{S30} on the x axis, with correlation coefficients (r) and p -value for each of the three models as stated in the legend. (b) $\ln(V_{S30})$ plotted on the x axis for each of the three models. (c) Site term versus V_{S30} for model D5 for the sites with measured V_{S30} separated from sites with proxy V_{S30} values. The color version of this figure is available only in the electronic edition.

terms in the GMPE—for geometrical spreading (a_4) and intrinsic attenuation parameter (a_5). These two coefficients are highly correlated; it is difficult in regression to fully separate them. We prefer a model that demonstrates a geometrical spreading coefficient (a_4), which is closer to observed values from simulations (-1.2 ; i.e., model F5, see more discussion later), and an intrinsic attenuation coefficient that is realistic considering the observed values of Q in the region. The typical formulation for amplitude decay from intrinsic anelastic attenuation is $\exp(-\frac{\pi R L}{Q\beta})$, yielding an approximation for a_5 of

$$a_5 \approx \frac{-\pi f}{Q\beta}, \quad (13)$$

or

$$Q \approx \frac{-\pi f}{a_5 \beta}. \quad (14)$$

Further details and previous applications of this approximation can be found in [Baltay and Beroza \(2013\)](#) and [Bostock et al. \(2015\)](#). Of course, for PGA at these small magnitudes, we do not know exactly what the frequency f is, but we expect it to be in the 3- to 20-Hz range. For the magnitudes we consider, between M 1 and 4, large corner frequencies coupled with high-frequency attenuation of the signal (i.e., f_{\max} or κ) implies the signals are relatively narrowband, so we expect PGA to come from this relatively narrow range of frequencies.

Several of the models considered herein have intrinsic attenuation coefficients $a_5 = \sim -0.006$, comparable to those featured in NGA-West2 GMPEs (e.g., [Bozorgnia et al., 2014](#)); substituting those into equation (14) for the 3- to 20-Hz range and assuming $\beta = 3.5$ km/s suggest Q -values from ~ 500 to ~ 3100 , much larger than what is typically observed in southern California ([Hauksson and Shearer, 2006](#)). However, in the preferred model F5, $a_5 = -0.02$ indicates lower Q -values of ~ 140 – 930 for assumed high frequencies of PGA for these small magnitudes, which is in closer agreement with observed values of Q in the region for the paths of these event to station pairs. We recognize the simplicity of approximating a_5 in this way because PGA does not necessarily come from a single frequency, but it does provide a physical basis for separating the two terms that are otherwise numerically correlated and gives us some insight into the physical plausibility of the chosen GMPE model.

In light of this, our preferred model F5 has a geometrical spreading coefficient a_4 of -1.2 , which we set *a priori*. Numerical simulations for our study region ([Frankel et al., 1990](#)) suggest that the geometrical spreading coefficient may be -1.2 or -1.3 . Ten of the other models considered have much stronger geometric spreading, whether fixed or inverted (near -1.7 or stronger), similar to the small-magnitude spreading coefficients from other GMPEs such as NGA-West2. Constraining both the geometrical spreading and intrinsic attenuation terms is difficult because these terms are highly correlated. In fact, many GMPE developers constrain these two terms independently, in a multistage approach (e.g., [Boore et al., 2014](#); [Thompson and Baltay, 2017](#)). The models with unrealistically strong geometric spreading ($a_4 \approx -1.7$ or stronger) also have unphysically weak intrinsic attenuation

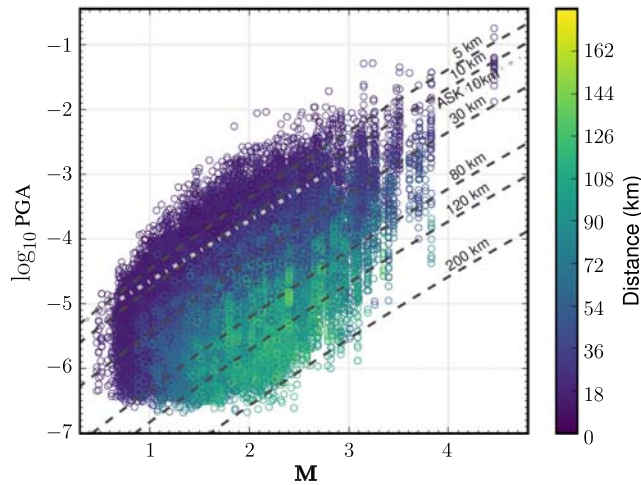


Figure 5. PGA data plotted with preferred model F5 at fixed distances. F5 is a model with geometrical spreading set *a priori* to -1.2 . Observations are shaded by R_{rup} , ground-motion prediction equation (GMPE) annotations next to their fixed distance line. ASK14 (Abrahamson *et al.*, 2014) is plotted at 10 km in light gray for comparison with the preferred GMPE. The color version of this figure is available only in the electronic edition.

terms ($a_5 \approx -0.006$), as discussed earlier. In light of the challenges, we particularly favor model F5 because its coefficients are more physically based. This is not an attempt to include more physics in the GMPE in a statistically robust fashion but to select a preferred model. This analysis has shown that there is more than one model that can fit the data equally well, and this method of discrimination may allow the final model to extrapolate to larger magnitudes and farther distances appropriately better than a model with less physical significance.

We plot models A5, D5, E5, and F5 for two distances (10 and 80 km) along with the results from prior studies (Abrahamson *et al.*, 2014; Baltay *et al.*, 2017; hereafter, ASK14 and BHA17, respectively; Fig. 6). The differences among models D5, E5, and F5 are minimal. The greatest difference is found among the three D5, E5, and F5 models and the least-squares model A5. This is likely because the mixed-effects models (D5, E5, and F5) solve for a median model in conjunction with the random effects, producing a more robust median model than the least-squares A5. In comparison with the ASK14 and BHA17 results, our models produce similar results with only slight differences between the intercept (between 0.5 and 1.0 \log_{10} units) and slope (difference of ~ 0.2). Our model F5 closely tracks ASK14 for magnitudes greater than 3, the magnitude range from which it was developed, and only diverges for the smaller magnitudes where it was not constrained. This gives us even more confidence in our model and suggests that it can be used in concert with ASK14 to predict smaller magnitude ground motions. Larger differences are observed with the BHA17 model, likely because of different development methods (BHA17 set a magnitude slope of 1.5 consistent with source physics) and a different dataset (a small-magnitude Anza-region dataset with recordings only

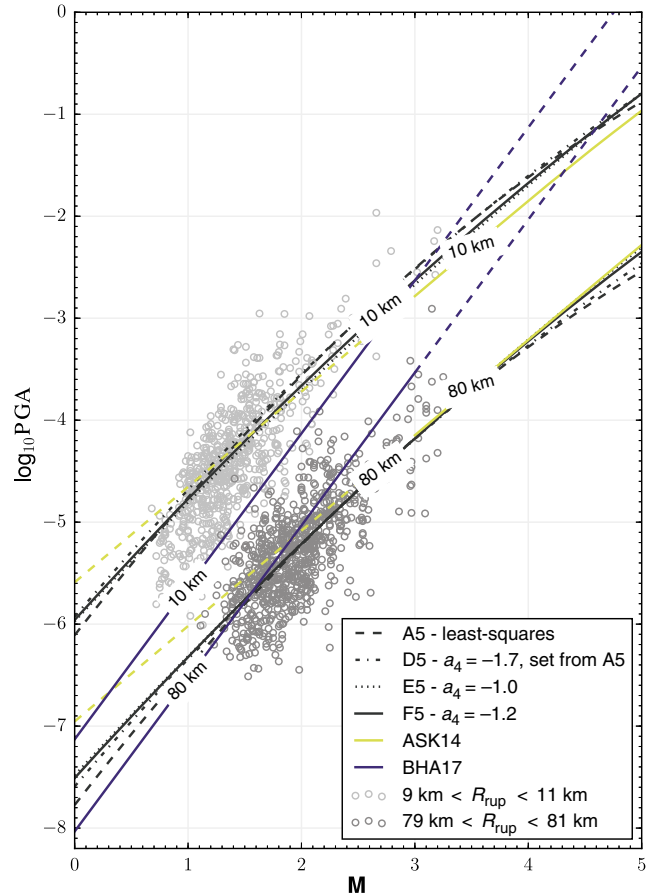


Figure 6. A comparison of four GMPEs presented here (models A5, D5, E5, and F5), along with those of ASK14, and Baltay *et al.* (2017; hereafter, BHA17). Black dashed line, model A5; black small dashed-dotted line, model D5, $a_4 = -1.7$ from model A5; black dotted line, model E5, $a_4 = -1.0$; black solid line, model F5, $a_4 = -1.2$; lighter gray line, ASK14; and darker gray line, BHA17. BHA17 and ASK14 lines are solid where constrained by data. Light-gray circles are all recordings with R_{rup} greater than 9 km and less than 11 km; medium-gray circles are all recordings with R_{rup} greater than 79 km and less than 81 km. The color version of this figure is available only in the electronic edition.

within 20 km in the case of BHA17). We also note that our small-magnitude GMPE continues to steepen with magnitude at smaller and smaller magnitudes, a physically desirable attribute as the slope approaches the theoretical limit of M 1.5 (Baltay and Hanks, 2014). We conclude that our model results are within the expected agreement with past studies but perhaps more tailored to the region and extrapolable with coefficients representative of the underlying physics.

Mixed-Effects MLE versus OLS Approach

The standard deviation of the event terms τ , is always lower in the MLE approach than the POLS method (Fig. 7a). Whereas events recorded on many stations (>25) produce similar event terms and uncertainties for both the POLS and mixed-effects methods, events recorded by few stations show large variation between the two approaches, with the

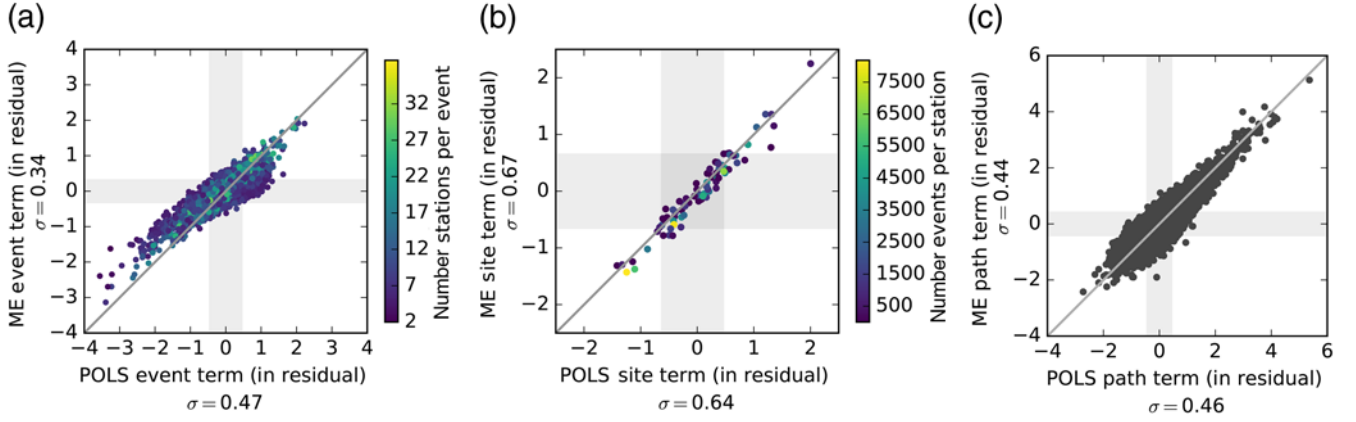


Figure 7. Mixed-effects versus single-mean residuals for models F5 versus A5. (a) Event terms, shaded by the number of stations that record each event. τ for each model denoted on the axes and hatched in the figure. (b) Site terms, shaded by the number of events recorded on each station. ϕ_S for each model denoted on the axes and hatched in the figure. (c) Path terms for each model. ϕ_P for each model denoted on the axes and hatched in the figure. Path terms are not shaded because this study does not classify them by similar paths. The color version of this figure is available only in the electronic edition.

mixed-effect value always being less (on an absolute scale, i.e., closer to 0) than the POLS value for that event term. This skewedness is a direct result of how the computational method solves for the random effects values. Abrahamson and Youngs (1992) outline an algorithm to compute the values of random effects (event terms) for a mixed-effects model with only a single random effect, without removing bias. This is an iterative algorithm, by which the uncertainties are first solved for, and then the random effects determined from these

$$\delta E_{i_ME} = \frac{\tau^2 \sum_{j=1}^{n_i} \delta_{ij}}{n_i \tau^2 + \phi^2}, \quad (15)$$

in which δE_{i_ME} is the mixed-effects method event term for earthquake i , δ_{ij} is the residual for each recording of earthquake i at station j , τ^2 is the variance of all event terms, ϕ^2 is the variance for all within-event terms, and n_i is the number of stations that record event i . We can express equation (15) using our original definition of the event term (equation 8) as

$$\delta E_{i_ME} = \frac{\delta E_{i_POLS}}{1 + \frac{1}{\tau^2 n_i} \phi^2}, \quad (16)$$

in which δE_{i_POLS} is the POLS event term for earthquake i . Thus, for n_i large (an event with many recordings), the denominator of equation (16) approaches 1, and the mixed-effect event-term approaches the single-mean event term because this event is better constrained. Rodriguez-Marek *et al.* (2013) and Kotha *et al.* (2017) note this relationship as well. This is exactly what we observe in Figure 7a, with δE_{i_POLS} for events recorded on many stations (lighter shades) becoming more similar to δE_{i_ME} . For less well-recorded events, the within-event uncertainty ϕ begins to influence the mixed-effect event term. The specific relationship between the two-event terms is governed not by the underlying distribution of event terms but by the distribution of the site and path terms because $\phi = \text{st.dev.}(\delta S_j + \delta P_{ij})$.

Similarly, if there are two random effects (event and site), then equation (15) becomes for an event term

$$\delta E_{i_ME} = \frac{\tau^2 \sum_{j=1}^{n_i} \ln(y_{ij}) - \mu_{ij}}{n_i \tau^2 + m_j \phi_S^2 + \phi_0^2}, \quad (17)$$

and for a site term

$$\delta S_{j_ME} = \frac{\phi_S^2 \sum_{i=1}^{m_j} \ln(y_{ij}) - \mu_{ij}}{n_i \tau^2 + m_j \phi_S^2 + \phi_0^2}, \quad (18)$$

in which δS_{j_ME} is the mixed-effects site term for station j , ϕ_S^2 is the variance for all site terms, ϕ_0^2 is the variance for all remaining residuals—path and aleatory, and m_j is the number of events recorded on station j . Of course, in this case, the random effects may still be represented as a function of the POLS event and site terms; for any given event i :

$$\delta E_{i_ME} = \frac{\tau_S^2 \delta E_{i_POLS}}{\tau^2 + \frac{1}{n_i} (\phi_S^2 + \phi_0^2)}, \quad (19)$$

and any given station j :

$$\delta S_{j_ME} = \frac{\phi_S^2 \delta S_{j_POLS}}{\phi_S^2 + \frac{1}{m_j} (\tau^2 + \phi_0^2)}, \quad (20)$$

in which both equations (19) and (20) can be found by taking equations (17) and (18) with $m_j = 1$ for any single given event and for any given station, $n_i = 1$.

Similarly, with a single random effect, for any event or site, if n_i or m_j is large, then respectively, the mixed-effects event or site terms will be closer in value to the POLS event or site term; for individuals less well constrained, the remaining uncertainty begins to affect the value of the random effect.

For the data we use in this study, there are significantly more events ($> 10,000$) than there are sites (~ 80). Therefore, for most stations, m_j will be much larger than n_i for any given event. Thus, the site terms show less variation in values between approaches than the event terms (Fig. 7). This figure also gives a rule of thumb for how many stations need to record an event before the two event estimates are similar: 10 or more stations seems to be sufficient here.

There are important implications for these findings, which can guide how to use these event, site, and path terms in future studies. For example, for any given earthquake, a POLS approach suggests that the event term (or parameter of interest) is the mean value of observations for that earthquake, which will always be between the minimum and maximum observed value. However, with a mixed-effects approach, the event term or parameter of interest could be predicted to be less than any of the observed values. This may be counterintuitive from a seismological perspective, but is statistically a more robust approach. A POLS approach, as we have set up here, assumes that the observations are independent; however, this is obviously not the case because recordings at the same station should be strongly correlated, as well as to some extent recordings of the same earthquake at different stations.

Mixed-effects models do not assume this and use random effects to compensate for biases derived from the selected population of variables in the dataset (in this application, the selected population of earthquakes and stations). This yields a better median model and includes an estimate of the random effects (or residuals that may be of interest to seismological applications). This is also reflected in the definition of an MLE (the backbone of the mixed-effects algorithm): the MLE maximizes the likelihood of any one observation being part of the underlying distribution (of fixed and random effects), while simultaneously estimating the uncertainty. An ordinary least-squares (OLS) algorithm (i.e., with no covariance) assumes that the data are normally distributed and simply minimizes the squared error. Further details of the implications of a POLS versus mixed-effects approach with regard to event terms and stress drops are planned to be released by coauthor Baltay and others.

Similarly, there are implications for site terms or site parameters. If there are on average many more recordings per earthquake than recordings per station, as in our study, the inversions place more uncertainty in the site term in the mixed-effects approach than the POLS approach, resulting in a slightly lower POLS site term than mixed-effects site term. In contexts with similar event-to-station data weights, POLS approaches place less variability in site terms than are realistic. To the contrary, in studies in which the number of stations outweigh the number of events, these results could be reversed, where the POLS method may place more variability in the site term than is warranted. In either case, the selection of the method used to compute these terms is an important consideration when interpreting the results, in particular if the residual values are of interest.

The path term in this study is not a random effect, so equations (15)–(20) do not apply to the computation thereof. The path terms are simply the remaining residuals between the observations and predictions from the GMPE plus random effects. Of course, because the mixed-effects approach attempts to find the maximum-likelihood solution for GMPE coefficients and random effects simultaneously, the overall model fit is better; the uncertainty in the path terms by definition will be smaller in the mixed-effects approaches than in the POLS approach. Although this is what we observe, the differences are small, showing only 0.03 between approaches. As such, the method used to obtain these path terms is not as important in the final analyses using the path terms and their uncertainties. Regardless, our results suggest that the mixed-effects approach is still the preferred solution to obtain path terms because the median model on which they are based will not be biased by random effects (the selected population of earthquakes and stations).

The differences between (and implications of) these two approaches are not new. The MLE approach has been widely used in ground motion and engineering seismology since the 1980s (Brillinger and Preisler, 1984, 1985; Abrahamson and Youngs, 1992). Some recently published studies in the ground-motion field have also compared the POLS and MLE approaches, with focuses on the resulting uncertainties between models (Stafford, 2014; Kotha *et al.*, 2016, 2017). However, the POLS approach remains integral in studies arising from the broader seismological community in obtaining event or site correction terms (Andrews, 1986; Allmann and Shearer, 2009; Kilb *et al.*, 2012). Because the ANZA seismic network and southern California region have long served as popular natural laboratory for many seismological source and structure studies and because the availability of seismological data here will only increase, we hope that this article may reach such an audience and augment such future studies.

Site Effects and V_{S30}

Finally, the results of this study show that the site terms do not correlate with V_{S30} . This is demonstrated in Figure 4, as well as in Figure 8, where the V_{S30} and site-term values for the stations in this dataset are plotted in map view. From Figure 4 and Table 1, it is evident that model D5, with no V_{S30} term, produces virtually the same values (within 0.01 natural log units) of site terms as model D6 (including an inverted V_{S30} term coefficient). The mixed-effects model D5 seems to compensate for the lack of a V_{S30} term by adjusting the intercept coefficient a_1 to produce the same site terms as model D6_site (for which the a_6 coefficient is inverted and very small) for the maximum-likelihood solution. The least-squares model A6 does not contain random effects in which to place any site residuals, so any site effects (V_{S30} -related or not) are placed in the a_6 coefficient instead of in a site term and adjusted a_1 coefficient. In model D6_site, where a_6 is set from the least-squares model, the mixed-effects inversion compensates for the unrealistic input V_{S30} relationship

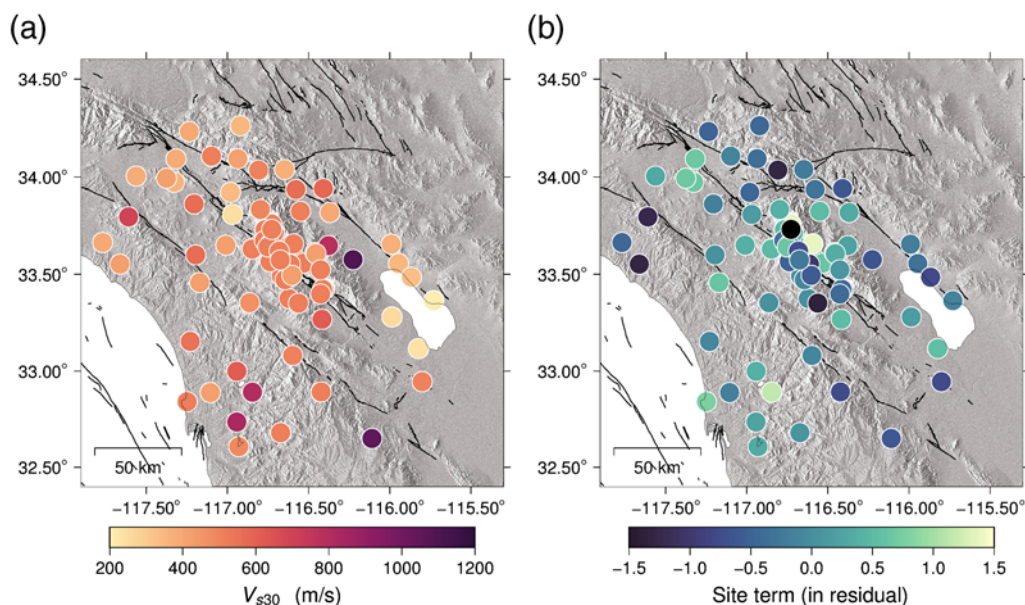


Figure 8. (a) Map view of V_{S30} for each station in the database; (b) map view of the site term for each station in the database from our favored model F5. A correlation between V_{S30} and site terms would imply that lower V_{S30} values (lighter shades in panel a) would correspond to higher ground motions or site terms (lighter shades in panel b). The color version of this figure is available only in the electronic edition.

by adjusting the site terms and thus the larger standard deviation of the unique site terms φ_S (Table 2).

There are several possibilities to explain the underlying causes of this null relationship between site terms and V_{S30} . We did not conduct a detailed investigation but suggest some possibilities, including:

1. The relatively homogeneous distribution of medium- to hard-rock V_{S30} values within the dataset (Fig. 2c), which makes a linear fit statistically difficult; an absence of large basins or sedimentary fill (the sediment at these sites being mainly surficial or very compacted sediment (Dibblee, 1954; Sharp, 1967). Some studies (Pulido and Matsuoka, 2006) suggested that in regions such as these, V_{S5} or V_{S10} may be a better measure of site effects.
2. The small-magnitude nature of the dataset (Fig. 2a) leading to mostly linear site effects, but V_{S30} may be most effective for studies with nonlinear response. This may be related to (1) as higher frequencies such because these would respond to shallower sheens of sediment over bedrock.
3. That the small magnitudes yield PGA at high frequencies, in which V_{S30} relationships have been observed to have an opposite sign (amplification for larger V_{S30}) than at lower frequencies (Steidl, 2000; Thompson and Wald, 2016).
4. Perhaps that, at least in this region, site effects may be derived from more than just near-surface characteristics. Kotha *et al.* (2016) noted that the correlation between site amplification and V_{S30} appeared to be region dependent.

Site effects here may be more representative of characteristics in some km^3 -wide volume surrounding the site (Fig. 8) in that they are reflecting near-site path effects. These results are not surprising because other studies have found

that V_{S30} is often not a robust estimate of site effects (Gallipoli and Mucciarelli, 2009) and that a better correlation between representation of site effects is often a combination of site-condition proxies such as V_{S30} and H_{800} (depth to 800 m/s; Derras *et al.*, 2016, 2017) or $Z_{1.0}$ (depth to 1.0 km/s). Derras *et al.* (2016, 2017) observed a lack of correlation between amplification and V_{S30} , though they found an improved correlation between these with measured V_{S30} as opposed to an inferred or proxy V_{S30} . We do not observe an improved correlation here (0.01 vs. -0.03). Finally, these results only show an absence of correlation between V_{S30} and PGA; however, a definitive study on site amplification and V_{S30} warrants an analysis of a broader frequency range.

In light of these site-term observations, we provide a table of PGA site-term corrections (our site residuals, Table 3), which may be used as corrections for studies interested in removing site effects. We expect this information will be useful for future studies that use southern California data and in particular ANZA (AZ) and Caltech (CI) network stations such as that of Kilb *et al.* (2012), who estimated kappa from similar magnitude earthquakes on ANZA stations, or Trugman and Shearer (2017), who decomposed spectra into source, site, and path components for small-magnitude events using some of the same stations to estimate earthquake stress drop. The high-frequency site terms as we publish here are very applicable and could be very useful for these types of studies. The provided terms in Table 3 are additive in units of $\ln(\text{PGA})$ and should only be used for events within the magnitude range of the model we have derived (Stafford *et al.*, 2017). This approach is becoming more common and has been shown to both reduce uncertainty and move toward partially nonergodic models (Rodriguez-Marek *et al.*, 2013; Landwehr *et al.*, 2016;

Table 3
Station Codes, Site Terms, and Standard Error (Std. Err.) for Peak Ground Acceleration (PGA) from This Study

Site	Term	Std. Err.	Site	Term	Std. Err.	Site	Term	Std. Err.
B082A	0.41	0.01	IWR	0.51	0.01	RSS	0.66	0.09
B086A	0.63	0.01	JEM	-0.11	0.01	RVR	0.67	0.03
B088A	0.00	0.01	JFN4	0.32	0.01	SAL	0.17	0.03
BAR	0.05	0.02	JFS4	-0.04	0.01	SBPX	-0.51	0.08
BBR	-0.45	0.04	JORD	-0.09	0.01	SDD	-1.31	0.20
BBS	-0.48	0.06	KNW	0.46	0.01	SDR	0.23	0.05
BCCC	1.13	0.01	LLS	0.24	0.20	SFTR	0.64	0.01
BOM	-0.14	0.06	LVA2	-1.37	0.01	SLB	-0.78	0.06
BOR	0.50	0.01	MGE	0.32	0.11	SLR	0.39	0.02
BZN	-0.06	0.01	MLS	0.31	0.10	SMER	0.62	0.02
CLT	0.66	0.11	MONP2	-0.78	0.01	SND	-1.02	0.01
CPE	-0.18	0.06	MSC	-0.22	0.01	SNO	-1.30	0.02
CRY	-0.52	0.01	MSJ	0.14	0.10	SOL	0.77	0.30
CTC	-0.20	0.04	MUR	0.03	0.04	STG	-0.46	0.13
DEV	-0.31	0.09	NSS2	-0.33	0.25	SVD	-0.13	0.03
DGR	0.39	0.01	OLP	0.32	0.09	SWS	-0.78	0.03
DNR	-0.07	0.01	PER	-0.18	0.03	TFRD	-0.59	0.01
DPP	0.38	0.03	PFO	0.82	0.01	TMSP	-0.71	0.02
EML	1.15	0.03	PLM	0.03	0.01	TOR	-0.66	0.01
ERR	0.55	0.04	PLS	-1.24	0.05	TPFO	0.35	0.01
FHO	-0.37	0.02	PMD	0.22	0.01	TR01	-0.46	0.01
FOST	1.36	0.01	PRAN	1.36	0.02	TR04	-0.42	0.01
FRD	-1.43	0.01	PSD	0.51	0.05	TRO	0.08	0.01
GOR	-0.09	0.09	RDM	0.48	0.01	WMC	-0.26	0.01
GVAR1	0.16	0.01	RHL	-0.33	0.01	WRDG	2.25	0.02
IKP	-0.63	0.02	RRSP	-0.60	0.01	WWC	-0.64	0.02

Barbour and Crowell, 2017; Kotha *et al.*, 2017; Ktenidou *et al.*, 2018). However, a caveat is that it may only be of use to studies using existing, well-recorded earthquakes unless an analysis as demonstrated by Kotha *et al.* (2017) is performed. Future work in this region is needed to develop measurable parameters that can be used for site corrections for potential site locations that do not yet have the earthquake recording density necessary to drive these values empirically.

Conclusions

We use a large database of earthquake recordings (>120,000 waveforms) to obtain a GMPE in southern California, applicable to small-magnitude events and specific for the local region. Although the GMPE was developed on this specific small-magnitude database ($0.5 \leq M \leq 4.5$), we ensured that the expected underlying physics in terms of the magnitude and distance scaling was appropriately represented. In this way, the model should extrapolate well to larger magnitudes or distances ranges. In search of a suitable regional GMPE, this study investigated the effects of a traditional POLS versus a mixed-effects MLE approach on computing event, site, and path residuals within a dataset. The results suggest that the method used to obtain these terms has significant implications for any studies examining uncertainties within these terms or event, site, or path parameters. We find that a mixed-effects approach is the best method for working

with ground-motion data, as well as other geophysical datasets for which independence may not be a suitable assumption. In this particular application, in which the path terms are treated as the remaining residual and not a random effect, we suggest that a mixed-effects approach is the best method for obtaining path terms because the median model will not be biased by the selected population of earthquakes and stations. The stations in this study do not show a correlation between PGA and V_{S30} , indicating that V_{S30} is not representative of site effects in this region. We provide a table of site terms that may be used as a correction in studies using PGA for these stations. Future studies in this region should perform similar analyses to find a GMPE and site terms for PGV and EAS, similar to the work of Bindi *et al.* (2017).

Data and Resources

This work used a database of recordings and parameters computed by Janine Buehler and Frank Vernon and the Scripps Institution of Oceanography. These waveform data are publicly available and posted by the Scripps ANZA network on the Incorporated Research Institutions for Seismology (IRIS) Data Management Center (www.iris.edu, last accessed January 2017); however, the processing of these data was performed at Scripps using Antelope and MATLAB. The flatfile including event and station location, event magnitude, distance, and peak ground acceleration (PGA) is included in the $\text{\textcircled{E}}$ electronic supplement. The authors used python and R to perform further analyses on these data and Generic Mapping Tools (GMT; Wessel and Smith, 1998) to create the maps featured here.

Acknowledgments

This work (V. J. S., J. S. B., F. L. V., D. K.) was supported by Pacific Gas and Electric (PG&E). The authors would like to thank internal reviewers Andrew Barbour and Morgan Moschetti, as well as Associate Editor Fabrice Cotton and an anonymous reviewer for their constructive feedback, which greatly improved the quality of this article. Additionally, the authors would like to thank Andy Barbour, David Boore, Brian Chiou, Nico Kuehn, and Eric Thompson for their time providing thoughtful discussion and feedback regarding mixed-effects models and computing them using R. Any use of trade, firm, or product names is for descriptive purposes only and does not imply endorsement by the U.S. Government.

References

- Abrahamson, N. A., and R. R. Youngs (1992). A stable algorithm for regression analysis using the random effects model, *Bull. Seismol. Soc. Am.* **82**, no. 1, 505–510.

- Abrahamson, N. A., W. J. Silva, and R. Kamai (2014). Summary of the ASK14 ground-motion relation for active crustal regions, *Earthq. Spectra* **30**, no. 3, 1025–1055.
- Al Atik, L., N. Abrahamson, J. J. Bommer, F. Scherbaum, F. Cotton, and N. Kuehn (2010). The variability of ground-motion prediction models and its components, *Seismol. Res. Lett.* **81**, no. 5, 794–801.
- Allam, A. A.-Z., Y. Ben-Zion, I. Kurzon, and F. L. Vernon (2014). Seismic velocity structure in the hot springs and trifurcation areas of the San Jacinto fault zone, *Geophys. J. Int.* **198**, no. 2, 978–999.
- Allmann, B. P., and P. M. Shearer (2009). Global variations of stress drop for moderate to large earthquakes, *J. Geophys. Res.* **114**, no. B01310, doi: [10.1029/2008JB005821](https://doi.org/10.1029/2008JB005821).
- Ameri, G., S. Drouet, P. Traversa, D. Bindi, and F. Cotton (2017). Toward an empirical ground motion prediction equation for France: Accounting for regional differences in the source stress parameter, *Bull. Earthq. Eng.* **15**, 4681–4717.
- Anderson, J. G., and J. N. Brune (1999). Probabilistic seismic hazard analysis without the ergodic assumption, *Seismol. Res. Lett.* **70**, no. 1, 19–28.
- Andrews, D. J. (1986). Objective determination of source parameters and similarity of earthquakes of different size, in *Earthquake Source Mechanics*, S. Das, J. Boatwright, and C. H. Scholz (Editors), Am. Geophys. Union, Washington, D.C.
- Atkinson, G. M. (2015). Ground-motion prediction equation for small-to-moderate events at short hypocentral distances, with application to induced-seismicity hazards, *Bull. Seismol. Soc. Am.* **105**, no. 2A, 981–992.
- Atkinson, G. M., and M. Morrison (2014). Observations on regional variability in ground-motion amplitudes for small-to-moderate earthquakes in North America, *Bull. Seismol. Soc. Am.* **99**, no. 4, 2393–2409.
- Baltay, A., and G. C. Beroza (2013). Ground-motion prediction from tremor, *Geophys. Res. Lett.* **40**, no. 24, 6340–6345.
- Baltay, A. S., and T. C. Hanks (2014). Understanding the magnitude dependence of PGA and PGV in NGA-West2 data, *Bull. Seismol. Soc. Am.* **104**, no. 6, 2851–2865.
- Baltay, A. S., T. C. Hanks, and N. Abrahamson (2017). Uncertainty, variability, and earthquake physics in ground-motion prediction equations, *Bull. Seismol. Soc. Am.* **107**, no. 4, 1754–1772.
- Barbour, A. J., and B. W. Crowell (2017). Dynamic strains for earthquake source characterization, *Seismol. Res. Lett.* **88**, no. 2A, 354–370.
- Bates, D., M. Maechler, B. Bolker, and S. Walker (2015). Fitting linear mixed-effects models using lme4, *J. Stat. Software* **67**, no. 1, 1–48.
- Bayless, J. R., and N. A. Abrahamson (2018). An empirical model for Fourier amplitude spectra using the NGA-West2 database, *2018 Seismol. Soc. of Am. Annual Meeting*, Miami, Florida, 15–17 May.
- Beauval, C., H. Tasan, A. Laurendeau, E. Delavaud, F. Cotton, P. Guéguen, and N. Kuehn (2012). On the testing of ground-motion prediction equations against small-magnitude data, *Bull. Seismol. Soc. Am.* **102**, no. 5, 1994–2007.
- Bennett, R. A., W. Rodi, and R. E. Reilinger (1996). Global Positioning System constraints on fault slip rates in southern California and northern Baja, Mexico, *J. Geophys. Res.* **101**, no. B10, 21,943–21,960.
- Berger, J., L. M. Baker, J. N. Brune, J. B. Fletcher, T. C. Hands, and F. L. Vernon (1984). The Anza array: A high-dynamic-range, broad-band, digitally-radiotelemetered, seismic array, *Bull. Seismol. Soc. Am.* **89**, 1469–1481.
- Beyer, K., and J. J. Bommer (2006). Relationships between median values and between aleatory variabilities for different definitions of the horizontal component of motion, *Bull. Seismol. Soc. Am.* **96**, no. 4, 1512–1522.
- Bindi, D., D. Spallarossa, and F. Pacor (2017). Between-event and between-station variability observed in the Fourier and response spectra domains: Comparison with seismological models, *Geophys. J. Int.* **210**, no. 2, 1092–1104.
- Bommer, J. J., and N. A. Abrahamson (2006). Why do modern probabilistic seismic-hazard analyses often lead to increased hazard estimates?, *Bull. Seismol. Soc. Am.* **96**, no. 6, 1967–1977.
- Boore, D. M. (2006). Orientation-independent, nongeometric-mean measures of seismic intensity from two horizontal components of motion, *Bull. Seismol. Soc. Am.* **100**, no. 4, 1830–1835.
- Boore, D. M., J. P. Stewart, E. Seyhan, and G. M. Atkinson (2014). NGA-West2 equations for predicting PGA, PGV, and 5% damped PSA for shallow crustal earthquakes, *Earthq. Spectra* **30**, no. 3, 1057–1085.
- Bostock, M. G., A. M. Thomas, A. M. Rubin, and N. I. Christensen (2015). Magnitudes and moment-duration scaling of low-frequency earthquakes beneath southern Vancouver Island, *J. Geophys. Res.* **120**, 6329–6350.
- Bozorgnia, Y. A., N. A. Abrahamson, L. Al Atick, T. D. Ancheta, G. M. Atkinson, J. W. Baker, A. Baltay, D. M. Boore, K. W. Campbell, B. S. J. Chiou, et al. (2014). NGA-West2 research project, *Earthq. Spectra* **30**, no. 3, 973–987.
- Brillinger, D. R., and H. K. Preisler (1984). An exploratory analysis of the Joyner-Boore attenuation data, *Bull. Seismol. Soc. Am.* **74**, no. 4, 1441–1450.
- Brillinger, D. R., and H. K. Preisler (1985). Further analysis of the Joyner-Boore attenuation data, *Bull. Seismol. Soc. Am.* **75**, no. 2, 611–614.
- Chiou, B., R. Youngs, N. Abrahamson, and K. Addo (2010). Ground-motion attenuation model for small-to-moderate shallow crustal earthquakes in California and its implications on regionalization of ground-motion prediction models, *Earthq. Spectra* **26**, no. 4, 907–926.
- Derras, B., P. Y. Bard, and F. Cotton (2016). Site-condition proxies, ground motion variability, and data-drive GMPEs: Insights from the NGA-West2 and RESORCE datasets, *Earthq. Spectra* **32**, no. 4, 2027–2056.
- Derras, B., P. Y. Bard, and F. Cotton (2017). V_{S30} , slope, H_{800} , and f_0 : Performance of various site-condition proxies in reducing ground-motion aleatory variability and predicting nonlinear site response, *Earth Planets Space* **69**, no. 1, 133.
- Dibblee, T. W., Jr. (1954). Geology of the Imperial Valley region, California, in *Geology of Southern California*, Bulletin 170, 21–28.
- Fang, H., H. Zhang, H. Yao, A. Allam, D. Zigone, and R. D. van der Hilst (2016). A new algorithm for three-dimensional joint inversion of body wave and surface wave data and its application to the Southern California plate boundary region, *J. Geophys. Res.* **121**, no. 5, 3557–3569.
- Frankel, A., A. McGarr, J. Bicknell, J. Mori, L. Seeber, and E. Cranswick (1990). Attenuation of high-frequency shear waves in the crust: Measurements from New York state, South Africa, and southern California, *J. Geophys. Res.* **95**, no. B11, 17,441–17,457.
- Gallipoli, M. R., and M. Mucciarelli (2009). Comparison of site classification from V_{S30} , V_{S10} , and HVSR in Italy, *Bull. Seismol. Soc. Am.* **99**, no. 1, 340–351.
- Greene, W. (2012). *Econometric Analysis*, Seventh Ed., Pearson Education, Inc, Saddle River, New Jersey.
- Gregor, N., N. A. Abrahamson, G. M. Atkinson, D. M. Boore, Y. Bozorgniz, K. Campbell, and B. Chiou (2014). Comparison of NGA-West2 GMPEs, *Earthq. Spectra* **30**, no. 3, 1179–1197.
- Hanks, T. C., and D. M. Boore (1984). Moment-magnitude relations in theory and practice, *J. Geophys. Res.* **89**, no. B7, 6229–6235.
- Hanks, T. C., N. A. Abrahamson, J. W. Baker, M. P. Board, D. M. Boore, J. N. Brune, C. A. Cornell, and J. W. Whitney (2013). Extreme ground motions and Yucca Mountain, *U.S. Geol. Surv. Open-File Rept. 2013-1245*.
- Hardebeck, J. L., and E. Hauksson (2001). Crustal stress field in southern California and its implications for fault mechanics, *J. Geophys. Res.* **106**, no. B10, 21,859–21,882.
- Hauksson, E., and P. Shearer (2006). Attenuation models (Q_p and Q_s) in three dimensions of the southern California crust: Inferred fluid saturation at seismogenic depths, *J. Geophys. Res.* **111**, no. B5, doi: [10.1029/2005JB003947](https://doi.org/10.1029/2005JB003947).
- Kilb, D., G. Biasi, J. Anderson, J. Brune, Z. Peng, and F. L. Vernon (2012). A comparison of spectral parameter kappa from small and moderate earthquakes using southern California ANZA seismic network data, *Bull. Seismol. Soc. Am.* **102**, no. 1, 284–300.
- Kotha, S. R., D. Bindi, and F. Cotton (2016). Partially non-ergodic region specific GMPE for Europe and Middle-East, *Bull. Earthq. Eng.* **14**, no. 4, 1245–1263.

- Kotha, S. R., D. Bindi, and F. Cotton (2017). From ergodic to region- and site-specific probabilistic seismic hazard assessment: Method development and application at European and Middle Eastern sites, *Earthq. Spectra* **33**, 1433–1453.
- Ktenidou, O. J., Z. Roumelioti, N. Abrahamson, F. Cotton, K. Pitilakas, and F. Hollender (2018). Understanding single-station ground-motion variability and uncertainty (σ): Lessons learnt from EUROSEISTEST, *Bull. Earthq. Eng.* **16**, no. 6, 2311–2336.
- Kurzon, I. F.-Z., F. L. Vernon, Y. Ben-Zion, and G. M. Atkinson (2014). Ground motion prediction equations in the San Jacinto fault zone: Significant effects of rupture directivity and fault zone amplification, *Pure Appl. Geophys.* **171**, no. 11, 3045–3081.
- Landwehr, N. N., N. M. Kuehn, T. Scheffer, and N. Abrahamson (2016). A nonergodic ground-motion model for California with spatially varying coefficients, *Bull. Seismol. Soc. Am.* **106**, no. 6, 2574–2583.
- Melgar, D., Y. Bock, and B. W. Crowell (2012). Real-time centroid moment tensor determination for large earthquakes from local and regional displacement records, *Geophys. J. Int.* **188**, no. 2, 703–718.
- Oth, A., H. Miyake, and D. Bindi (2017). On the relation of earthquake stress drop and ground motion variability, *J. Geophys. Res.* **122**, 5474–5492.
- Pinheiro, J. C., and D. Bates (2000). *Mixed Effects Models in S and S-PLUS*, Springer-Verlag, New York, New York.
- Plesch, A., J. H. Shaw, W. A. Bryant, S. Carena, M. L. Cooke, J. F. Dolan, G. Fuis, E. Gath, L. Grant, and E. Hauksson (2007). Community fault model for southern California, *Bull. Seismol. Soc. Am.* **97**, no. 6, 1793–1802.
- Pulido, N., and M. Matsuoka (2006). Broadband strong motion simulation of the 2004 Niigata-ken Chuetsu earthquake: Source and site effects, *Third International Symposium on the Effects of Surface Geology on Seismic Motion*, Grenoble, France, Vol. 1, 657–666.
- Richter, C. F. (1935). An instrumental earthquake magnitude scale, *Bull. Seismol. Soc. Am.* **25**, no. 1, 1–32.
- Rodriguez-Marek, A., F. Cotton, N. Abrahamson, S. Akkar, L. Al-Atik, B. Edwards, G. Montalva, and H. Dawood (2013). A model for single-station standard deviation using data from various tectonic regions, *Bull. Seismol. Soc. Am.* **103**, no. 6, 3149–3163.
- Ross, Z. E., Y. Ben-Zion, M. C. White, and F. L. Vernon (2016). Analysis of earthquake body wave spectra for potency and magnitude values: Implications for magnitude scaling relations, *Geophys. J. Int.* **207**, no. 2, 1158–1164.
- Sahakian, V. J., A. S. Baltay, T. C. Hanks, J. S. Buehler, F. L. Vernon, and D. Kilb (2016). Reducing uncertainty in GMPEs through physical explanations of the path term, presented at the *2016 Fall Meeting, AGU*, San Francisco, California, 12–16 December, Abstract S31C–793.
- Seyhan, E., and J. P. Stewart (2014). Semi-empirical nonlinear site amplification from NGA-West2 data and simulations, *Earthq. Spectra* **30**, no. 3, 1241–1256.
- Sharp, R. V. (1967). San Jacinto fault zone in the Peninsular Ranges of southern California, *Geol. Soc. Am. Bull.* **78**, no. 6, 705–730.
- Shaw, J. H., A. Plesch, C. Tape, M. Suess, T. H. Jordan, G. Ely, E. Hauksson, J. Tromp, T. Tanimoto, R. Graves, et al. (2015). Unified structural representation of the southern California crust and upper mantle, *Earth Planet. Sci. Lett.* **415**, 1–15.
- Stafford, P. J. (2014). Crossed and nested mixed effects approaches for enhanced model development and removal of the ergodic assumption in empirical ground motion models, *Bull. Seismol. Soc. Am.* **104**, no. 2, 702–719.
- Stafford, P. J., A. Rodriguez-Marek, B. Edwards, P. Kruiver, and J. Bommer (2017). Scenario dependence of linear site-effect factors for short-period response spectral ordinates, *Bull. Seismol. Soc. Am.* **107**, no. 6, 2859–2872.
- Steidl, J. (2000). Site response in southern California for probabilistic seismic hazard analysis, *Bull. Seismol. Soc. Am.* **90**, no. 6B, S149–S169.
- Thompson, E., and A. Baltay (2017). Mean rupture distances should replace minimum rupture distances, *Bull. Seismol. Soc. Am.* doi: [10.1785/0120170306](https://doi.org/10.1785/0120170306).
- Thompson, E., and D. Wald (2016). Uncertainty in V_{S30} -based site response, *Bull. Seismol. Soc. Am.* **106**, no. 2, 453–463.
- Trugman, D. T., and P. M. Shearer (2017). Application of an improved spectral decomposition method to examine earthquake source scaling in southern California, *J. Geophys. Res.* **122**, 2890–2910, doi: [10.1002/2017JB013971](https://doi.org/10.1002/2017JB013971).
- Vernon, F. L. (1989). Analysis of data recorded on the ANZA seismic network, *Ph.D. Dissertation*, University of California at San Diego.
- Walling, M. (2009). Non-ergodic probabilistic seismic hazard analysis and spatial simulation of variation in ground motion, *Ph.D. Dissertation*, UC Berkeley, Berkeley, California.
- Wang, F., and T. H. Jordan (2014). Comparison of probabilistic seismic-hazard models using averaging-based factorization, *Bull. Seismol. Soc. Am.* **104**, no. 3, 1230–1257, doi: [10.1785/0120130263](https://doi.org/10.1785/0120130263).
- Wessel, P., and W. H. Smith (1998). New, improved version of Generic Mapping Tools released, *Eos Trans. AGU* **79**, no. 47, 579.
- Yong, A., S. E. Hough, J. Iwahashi, and A. Braverman (2012). A terrain-based site-conditions map of California with implications for the contiguous United States, *Bull. Seismol. Soc. Am.* **102**, no. 1, 114–128.
- Yong, A., E. M. Thompson, D. Wald, K. L. Knudsen, J. K. Odum, W. J. Stephenson, and S. Haefner (2016). Compilation of V_{S30} data for the United States, *U.S. Geol. Surv. Data Series 978*, 8 pp., doi: [10.3133/ds978](https://doi.org/10.3133/ds978).

Earthquake Science Center
U.S. Geological Survey
345 Middlefield Road, MS 977
Menlo Park, California 94025
vjs@uoregon.edu
(V.S., A.B., T.H.)

Scripps Institution of Oceanography
University of California San Diego
9500 Gilman Drive
La Jolla, California 92039
(J.B., F.V., D.K.)

Civil and Environmental Engineering
UC Berkeley
447 Davis Hall
Berkeley, California 94720
(N.A.)

Manuscript received 13 December 2017;
Published Online 24 July 2018